

Supporting Information

Consecutive Junction-induced Efficient Charge Separation Mechanisms for High Performance MoS₂/Quantum Dot Phototransistors

Sangyeon Pak,^{a,†} Yuljae Cho,^{a,†} John Hong,^a Juwon Lee,^a Sanghyo Lee,^a Bo Hou,^a Geon-Hyoung An,^a Young-Woo Lee,^b Jae Eun Jang,^c Hyunsik Im,^d Stephen M. Morris,^a Jung Inn Sohn,^{d,} SeungNam Cha,^{a,e,*} Jong Min Kim^f*

^a Department of Engineering Science, University of Oxford, Parks Road, Oxford, OX1 3PJ, United Kingdom

^b Department of Energy Systems, Soonchunhyang University, Asan, Chungcheongnam-do, 31538, Republic of Korea

^c Department of Information and Communication Engineering, Daegu Gyeongbuk Institute of Science and Technology (DGIST), Daegu, 711-873, Republic of Korea

^d Division of Physics and Semiconductor Science, Dongguk University, Seoul 04620, Republic of Korea

^e Department of physics, Sungkyunkwan University, Suwon, Gyeonggi-do, 16419, Republic of Korea

^f Electrical Engineering Division, Department of Engineering, University of Cambridge, 9 JJ Thomson Avenue, Cambridge, CB3 0FA, United Kingdom

[†] S. Pak and Y. Cho contributed equally to this work.

* Corresponding author.

E-mail address: junginn.sohn@dongguk.edu, chasn@skku.edu / seungnam.cha@eng.ox.ac.uk

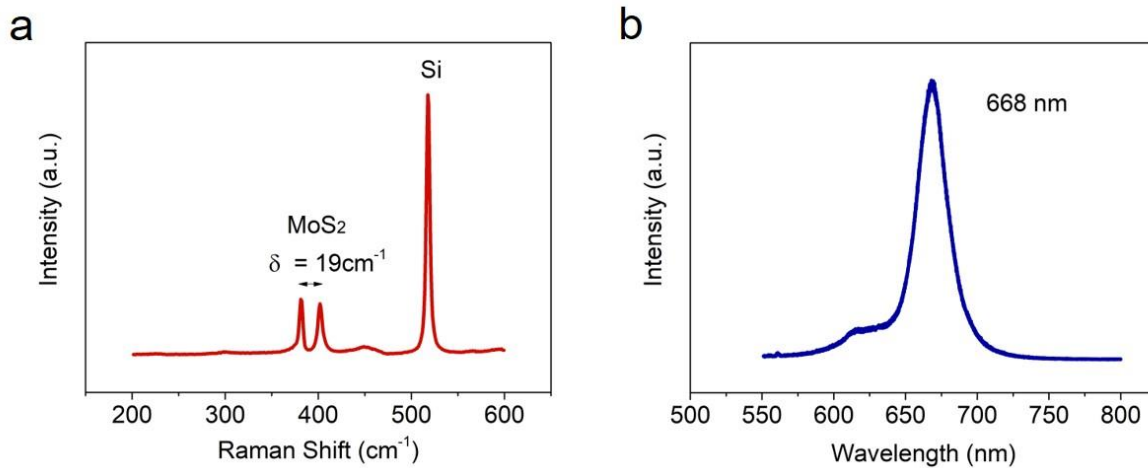


Figure S1. (a) Raman and (b) PL measurements of a MoS₂ monolayer.

To confirm the crystal quality of the CVD-grown MoS₂ monolayer, Raman and PL measurements were performed. For the pristine MoS₂, two characteristic peaks were observed at 382 cm⁻¹ and 401 cm⁻¹, which represent in-plane (E_{2g}^1) and out-of-plane vibrational modes (A_{1g}), respectively. The difference between the two peaks can be used to confirm the number of MoS₂ layers. The measured difference was close to 19 cm⁻¹, which implies that the synthesized MoS₂ is a monolayer. Photoluminescence measurement shows a strong PL peak centered at 668 nm. The strong PL intensity also confirms that the synthesized MoS₂ is a monolayer with a direct band gap.

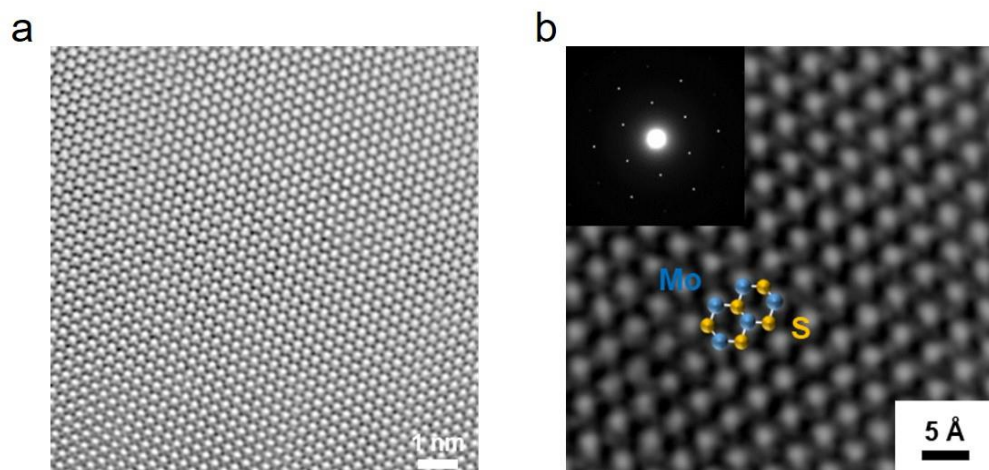


Figure S2. (a) High-resolution TEM image and (b) ADF-STEM image of a MoS₂ monolayer, representing the high crystallinity of the MoS₂ monolayer with a hexagonal structure. The bright spots correspond to the Mo atoms and the grey spots represent the S atoms. The inset shows an SAED image.

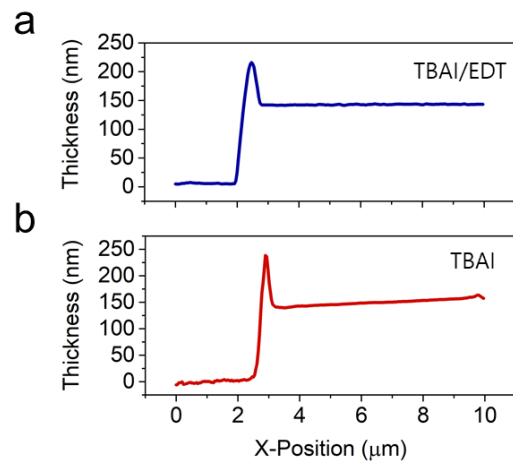


Figure S3. The step height of a) the 4 layers of TBAI-PbS with 2 layers of EDT PbS and b) the 6 layers of TBAI-PbS. The step height profile shows that the measured thickness of both QD films to be around 150 nm.

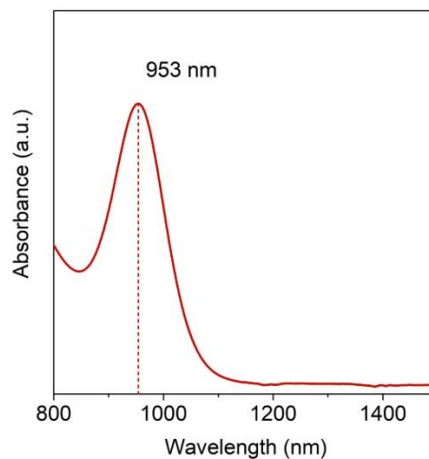


Figure S4. Absorption spectra of PbS QDs in toluene at a concentration of 50 mgmL^{-1} with the first absorption peak is observed at a wavelength of 953 nm.

The absorption spectrum of PbS CQDs in a solution phase were obtained over the range from 400 to 1500 nm using Ultraviolet–visible spectroscopy (UV-Vis). The first exciton peak was observed at 953 nm, which corresponds to a bandgap of 1.30 eV according to Planck-Einstein equation, $E = hc/\lambda$ where h is a Planck constant, c is the speed of light in a vacuum, and λ is the wavelength.

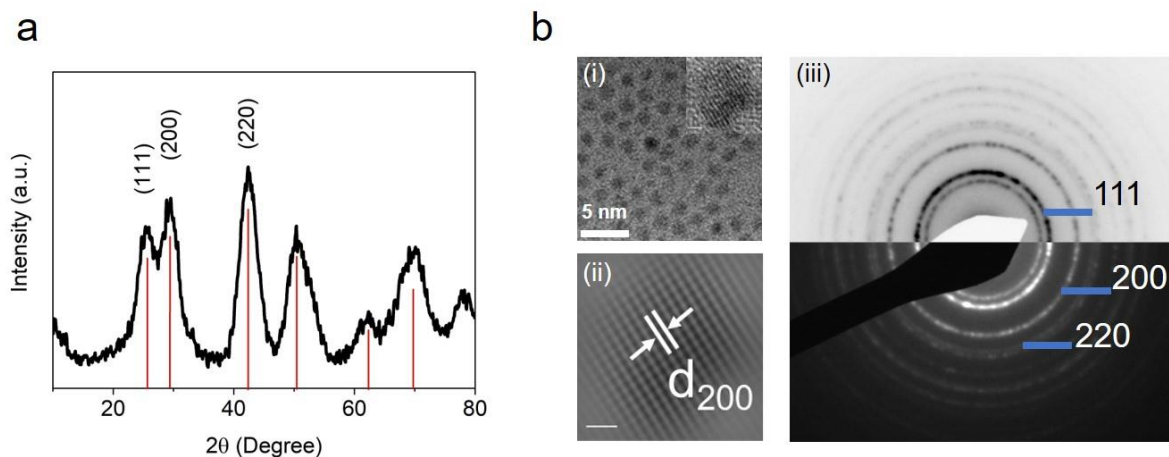


Figure S5. (a) XRD spectrum of a PbS CQDs layer passivated by oleic acid (OA). (b) (i) An HRTEM image of OA-passivated PbS CQDs (Scale bar: 5 nm). (ii) A magnified image of the PbS CQDs (Scale bar: 1 nm). (iii) SAED patterns of the PbS CQDs.

Crystallographic characterization of the as-synthesized PbS CQDs was performed using X-ray diffraction (XRD), high-resolution TEM (HRTEM), and selected area diffraction (SAED). As shown in Figures S6a,b, the typical rock-salt cubic crystalline structure (fcc) of the PbS CQDs was identified, which exhibits x-ray diffractions peaks due to the (111), (200), and (220) planes

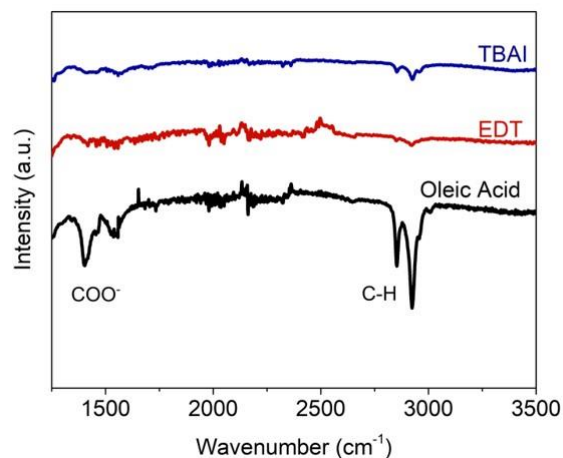


Figure S6. Surface analysis of the PbS CQDs passivated by Oleic Acid (Black), EDT (Red), and TBAI (Blue) using Fourier transform infrared (FT-IR) spectroscopy.

Characterization of the FT-IR spectra was performed to provide direct evidence of the removal of oleic acid (OA) from the PbS CQDs surface via an exchange with the EDT and TBAI ligands. The absence of the C–H and COO⁻ absorption peaks at around 3,000 cm⁻¹ and 1400 cm⁻¹, respectively, indicate that the OA that was originally on the PbS QD surface has been successfully replaced with the respective ligands (EDT or TBAI).

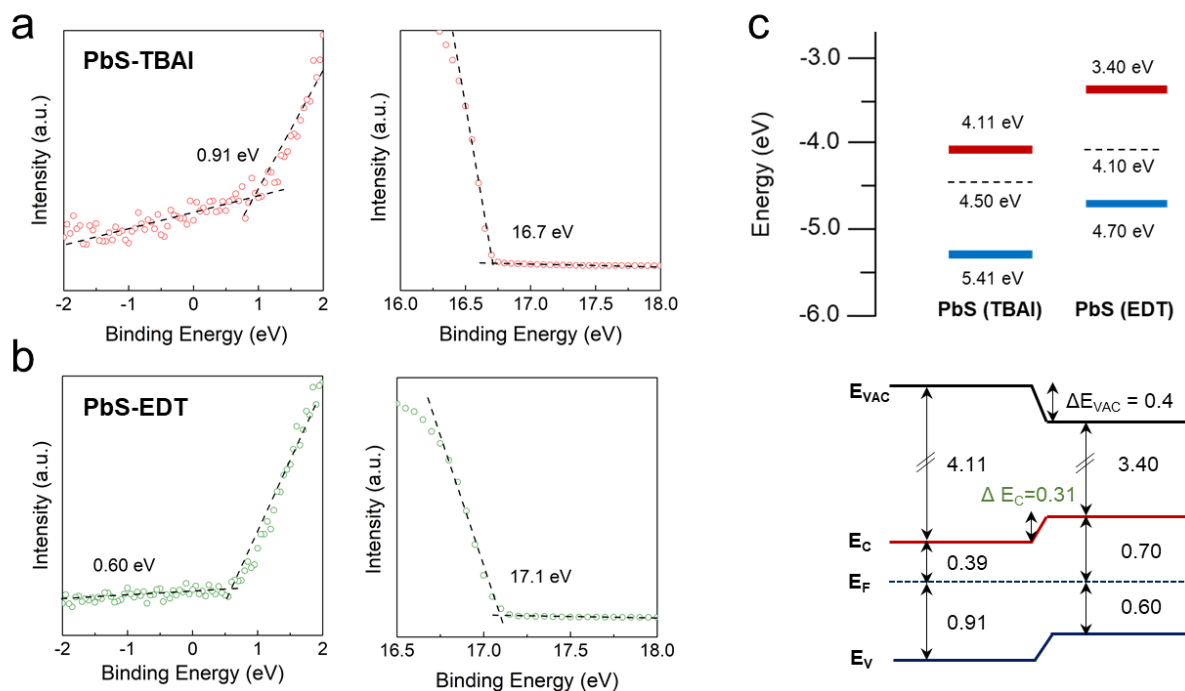


Figure S7. Ultraviolet photoelectron spectroscopy (UPS) measurements of PbS QDs with either TBAI or EDT ligands and the corresponding band alignment. (a,b) UPS spectra of a PbS QD film treated with either TBAI or EDT ligands. The cut-off binding energy of the PbS QD film is 16.7 (17.1) eV, and this corresponds to a work function of 4.50 (4.10) eV. (c) A diagram depicting the calculated energy levels of the PbS QDs treated with either TBAI or EDT ligands. The lower diagram in the figure depicts the energy band alignment for the PbS QDs treated with both TBAI and EDT ligands, confirming the presence of a large built-in potential of 0.31 eV.

In order to determine the Fermi level (E_F) and the valence band maximum (E_V) of the PbS QD layers with respect to the vacuum level, ultraviolet photoelectron spectroscopy (UPS) with a He source (21.2 eV) was employed. As shown in Figures S7a,b, the lower and upper binding energy edge are obtained using UPS measurements. The work function (ϕ) is calculated by subtracting the incident photon energy (21.2 eV) from the binding energy of the secondary electron cut-off (high binding energy edge). The work function with respect to E_{VAC}

of a TBAI-treated and EDT-treated PbS QD layer is calculated to be 4.50 eV (21.2 eV – 16.7 eV), and 4.10 (21.2 eV – 17.1 eV). The valence band maximum is determined by the difference between E_F and the lower binding energy edge measured from Figures S7a,b. Finally, the conduction band minimum (E_C) is calculated by adding the bandgap of the PbS QDs to the valence band maximum. The top image of Figure S7c illustrates the extracted energy levels from Figure S7a,b, and the bottom image illustrates the energy band diagram of a QD junction formed between TBAI- and EDT-treated PbS QDs layers.

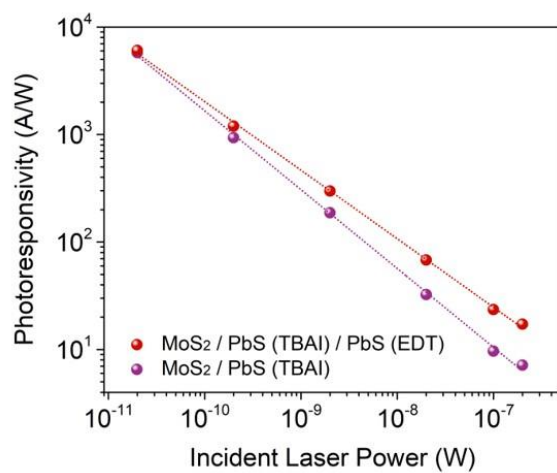


Figure S8. Photoresponsivity of a MoS₂/TBAI and a MoS₂/TBAI/EDT device with respect to the incident laser power.

Table S1. Performance of photodetectors based on MoS₂ and its hybrid structures.

Reference	Materials		Laser (nm)	Photoresponsivity (A/W)	Detectivity (Jones)	Rise Time (s)	Decay Time (s)
[1]	Exf. 1L MoS ₂		561	880	-	4	9
[2]	CVD 1L MoS ₂		450	178	-	>30	
[3]	Exf. >2L MoS ₂	PbS	635	10 ⁶	5 x 10 ¹⁴	-	0.35
[4]	Exf. 1-10L MoS ₂	TiO ₂ /PbS	635	~10 ⁵	5 x 10 ¹²	-	0.012
[5]	Exf. few layer MoS ₂	HgTe	600 – 2000	up to 10 ⁶	10 ¹²	-	0.004
[6]	Exf. thick MoS ₂	MAPbI ₃	500	10 ² -10 ³	10 ¹¹	0.025	0.05
This work	CVD 1L MoS₂	n-PbS/p-PbS	850	5 x 10⁴	10¹¹	0.00095	0.001

Supplementary References

- [1] Lopez-Sanchez, O.; Lembke, D.; Kayci, M.; Radenovic, A.; Kis, A. Ultrasensitive Photodetectors based on Monolayer MoS₂. *Nat. Nanotechnol.* **2013**, *8*, 497-501.
- [2] Lee, J.; Pak, S.; Giraud, P.; Lee, Y. -W.; Cho, Y.; Hong, J.; Jang, A. -R.; Chung, H. -S.; Hong, W. -K.; Jeong, H. Y.; Shin, H. S.; Occhipinti, L. G.; Morris, S. M.; Cha, S.; Sohn, J. I.; Kim, J. M. Thermodynamically Stable Synthesis of Large-Scale and Highly Crystalline Transition Metal Dichalcogenide Monolayers and their Unipolar n-n Heterojunction Devices. *Adv. Mater.* **2017**, *29*, 1702206.
- [3] Kufer, D.; Nikitskiy, I.; Lasanta, T.; Navickaite, G.; Koppens, F. H. L.; Konstantatos, G. Hybrid 2D-0D MoS₂-PbS Quantum Dot Photodetectors. *Adv. Mater.* **2015**, *27*, 176-180.
- [4] Kufer, D.; Lasanta, T.; Bernechea, M.; Koppens, F. H. L.; Konstantatos, G. Interface Engineering in Hybrid Quantum Dot-2D Phototransistors. *ACS Photonics* **2016**, *3*, 1324-1330.
- [5] Huo, N.; Gupta, S.; Konstantatos, G. MoS₂-HgTe Quantum Dot Hybrid Photodetectors beyond 2 μm. *Adv. Mater.* **2017**, *29*, 1606576.
- [6] Wang, Y.; Fullon, R.; Acerce, M.; Petoukhoff, C. E.; Yang, J.; Chen, C.; Du, S.; Lai, S. K.; Lau, S. P.; Voiry, D.; O'Carroll, D.; Gupta, G.; Mohite, A. D.; Zhang, S.; Zhou, H.; Chhowalla, M. Solution-Processed MoS₂/Organolead Trihalide Perovskite Photodetectors. *Adv. Mater.* **2017**, *29*, 1603995.